

XMM–Newton observations of PSR B1259–63 near the 2004 periastron passage

M. Chernyakova,^{1,2★†} A. Neronov,^{1,2} A. Lutovinov,³ J. Rodriguez⁴ and S. Johnston⁵

¹*INTEGRAL Science Data Center, Chemin d’Écogia 16, 1290 Versoix, Switzerland*

²*Geneva Observatory, 51 ch. des Maillettes, CH-1290 Sauverny, Switzerland*

³*Space Research Institute, 84/32 Profsoyuznaya Street, Moscow 117997, Russia*

⁴*CEA Saclay, DSM/DAPNIA/Service d’Astrophysique (CNRS UMR 7158 AIM), 91191 Gif sur Yvette, France*

⁵*Australia Telescope National Facility, CSIRO, PO Box 76, Epping, NSW 1710, Australia*

Accepted 2005 December 30. Received 2005 December 12; in original form 2005 June 4

ABSTRACT

PSR B1259–63 is in a highly eccentric 3.4-yr orbit with a Be star and crosses the Be star disc twice per orbit, just prior to and just after periastron. Unpulsed radio, X-ray and gamma-ray emission observed from the binary system is thought to be due to the collision of pulsar wind with the wind of Be star. We present here the results of new *XMM–Newton* observations of the PSR B1259–63 system during the beginning of 2004 as the pulsar approached the disc of the Be star. We combine these results with the earlier unpublished X-ray data from *BeppoSAX* and *XMM–Newton* as well as with the *ASCA* data. The detailed X-ray light curve of the system shows that the pulsar passes (twice per orbit) through a well-defined Gaussian-profile disc with the half-opening angle (projected on the pulsar orbit plane) $\Delta\theta_{\text{disc}} \simeq 18^\circ.5$. The intersection of the disc middle plane with the pulsar orbital plane is inclined at $\theta_{\text{disc}} \simeq 70^\circ$ to the major axis of the pulsar orbit. Comparing the X-ray light curve to the TeV light curve of the system, we find that the increase of the TeV flux some 10–100 d after the periastron passage is unambiguously related to the disc passage. At the moment of entrance to the disc, the X-ray photon index hardens from $\Gamma \simeq 1.8$ up to $\simeq 1.2$ before returning to the steeper value $\Gamma \geq 1.5$. Such behaviour is not easily accounted for by the model in which the X-ray emission is synchrotron emission from the shocked pulsar wind. We argue that the observed hardening of the X-ray spectrum is due to the inverse-Compton or bremsstrahlung emission from 10–100 MeV electrons responsible for the radio synchrotron emission.

Key words: pulsars: individual: PSR B1259–63 – X-rays: binaries – X-rays: individual: PSR B1259–63.

1 INTRODUCTION

PSR B1259–63 is a ~ 48 ms radio pulsar in a highly eccentric ($e \sim 0.87$), 3.4-yr orbit with a Be star SS 2883 (Johnston et al. 1992). The system’s distance from the Earth is $d \sim 2$ kpc (Johnston et al. 1994), note, however, that d is uncertain by a factor of ~ 2 based on radio measurements (see, e.g. Taylor, Manchester & Lyne 1993).

Be stars are well known to be the sources of strong highly anisotropic matter outflow. Both a dilute polar wind and a denser equatorial disc have been invoked to reconcile models for infrared, ultraviolet and optical observations (Waters et al. 1988). Timing analysis of the PSR B1259–63 system shows that the disc of Be star is tilted with respect to the orbital plane (Wex et al. 1998; Wang,

Johnston & Manchester 2004). The properties of the radio emission from the system are very different close to and far from the periastron. Radio observations of the 1994, 1997 (Johnston et al. 1999), 2000 (Connors et al. 2002), and 2004 (Johnston et al. 2005) periastron passages show that when the pulsar is far from the periastron, the observed radio emission is comprised entirely in highly linearly polarized pulsed emission from the pulsar itself with an intensity practically independent of the pulsar orbital position (McClure-Griffiths et al. 1998). But, starting about 100 d before periastron, depolarization of the pulsed emission occurs, the dispersion measure and the absolute value of the rotation measure increase while the flux density decreases. The pulsed radio emission then disappears entirely as the pulsar enters the disc and is hidden behind it (relative to the observer) approximately 20 d before the periastron passage. Shortly before the disc crossing, unpulsed radio emission appears and within several days sharply rises to a peak which is more than 10 times higher than the intensity of the pulsed emission far from

★E-mail: Masha.Chernyakova@obs.unige.ch

†M. Chernyakova is on leave from Astro Space Center of the P. N. Lebedev Physical Institute, Moscow, Russia

the periastron. Afterward, the unpulsed flux slightly decreases, as the pulsar passes through the periastron before reaching a second peak just after the pulsar crosses the disc for the second time. The unpulsed radio emission is detected until at least 100 d after the periastron passage. (Johnston et al. 1999, 2005; Connors et al. 2002).

The first detection of the X-rays from the PSR B1259–63 system was done by *ROSAT* in 1992 (Cominsky, Roberts & Johnston 1994). The most recent published observations of the system in X-rays were carried out with the *ASCA* satellite in 1994 and 1995 (Kaspi et al. 1995; Hirayama et al. 1999). These observations show that the X-ray emission is approximately twice as high at the time of the disc crossing than at periastron. In soft gamma-rays, the system was observed only after the periastron passage with *Compton Gamma-ray Observatory (CGRO)*/OSSE and *INTEGRAL*/ISGRI (Grove et al. 1995; Shaw et al. 2004). The combined soft gamma- and X-ray spectrum is consistent with a power law of photon index ~ 1.7 . This index also coincides with the radio spectral index of the unpulsed emission. No pulsed X-ray emission was detected from the system. With the standard epoch-folding method, the upper limit to a pulsed component in 2–10 KeV energy range was estimated to be about 10 per cent of the unpulsed component close to the periastron, and to about 40 per cent during the apastron (Kaspi et al. 1995; Hirayama et al. 1999). Note that the search for the pulsations in $P-\dot{P}$ space allowed Kaspi et al. (1995) to reduce an upper limit close to the periastron to less than 2 per cent under a certain assumption on the shape of pulse profile.

The 2004 periastron passage was observed in TeV gamma-rays by High Energy Stereoscopic System (HESS; Aharonian et al. 2005). TeV light curve of the source shows an unexpected behaviour. Contrary to the prediction that the TeV flux should be maximum at the periastron (Kirk, Skjæraasen & Gallant 2002), the flux apparently has a local minimum around this moment.

Several theoretical models were put forward to explain the behaviour of the X-ray light curve of the system. In the model of Tavani & Arons (1997), the enhancement of *synchrotron* X-ray emission during the disc passage is attributed to the enhancement of the magnetic field at the position of the contact surface of pulsar and stellar winds. In the model of Chernyakova & Illarionov (1999, 2000), the enhancement of the *inverse-Compton* X-ray emission during the disc passage is supposed to be due to the effect of the macroscopic mixing of the stellar and pulsar winds in the disc which effectively enhances the escape time of high-energy electrons responsible for the observed emission.

Typical energies of electrons responsible for the X-ray emission are $E_e \sim \text{TeV}$ in the Tavani & Arons (1997) model, while in the Chernyakova & Illarionov (1999) model $E_e \sim 10 \text{ MeV}$. One can, in principle, distinguish between the two models by comparing the details of radio, X-ray and TeV light curve of the system. We have organized a cycle of five *XMM-Newton* observations as the pulsar approached the 2004 periastron. In this paper, we present the results of our observations along with other *XMM-Newton* observations of the system not previously published. For the completeness, we also include the analysis of the previously unpublished *BeppoSAX* data. The 2004 periastron passage was extensively observed in radio (Johnston et al. 2005) and TeV (Aharonian et al. 2005) bands. Combination of the radio, X-ray and TeV data opens up a possibility, to study the evolution of the spectrum of PSR B1259–63 system over some 12 decades in energy.

Our analysis of large X-ray data set enables, for the first time, to constrain the geometrical parameters of the disc of Be star, such as the opening angle and orientation. Comparing the TeV and X-ray light curves, we find that the increase of the TeV flux some 10 to

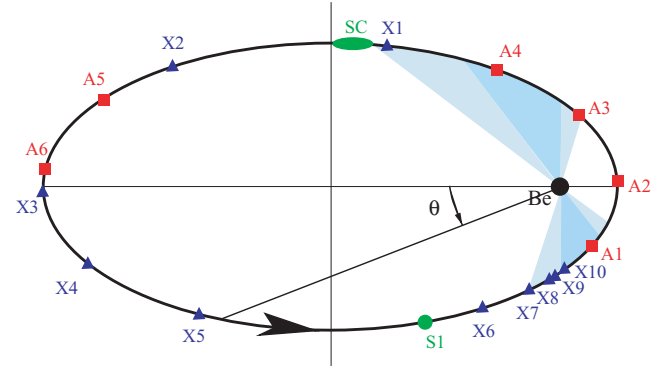


Figure 1. Schematic representation of the PSR B1259–63 binary system with the locations of the pulsar during the *XMM-Newton*, *BeppoSAX* and *ASCA* observations. Shaded area shows the geometry of the disc inferred from the X-ray data. Darker and lighter shaded regions correspond to one and two half-opening angles of the disc, respectively. Angle θ is the orbital phase of the pulsar referred in the text.

100 d after the periastron passage is unambiguously related to the pulsar passage through the Be star disc for the second time. This challenges the conventional interpretation of the observed TeV emission as the inverse-Compton emission from the pulsar wind electrons.

Another surprising result of our analysis that is not predicted in the theoretical models cited above is the persistently hard X-ray spectrum (photon index $\Gamma \simeq 1.2\text{--}1.3$) observed during the 10-d period when the pulsar enters the disc.

This paper is organized as follows. In Section 2, we describe the details of the *XMM-Newton* and *BeppoSAX* data analysis. The results are presented in Section 3, and discussed in Section 4.

2 OBSERVATIONS AND DATA ANALYSIS

In Fig. 1, we show a schematic drawing of the pulsar orbit along with the approximate location of the pulsar position during the *XMM-Newton*, *BeppoSAX*, and *ASCA* observations. The X-ray observations are more-or-less homogeneously distributed over the whole range of pulsar orbital phase $0 \leq \theta < 360^\circ$. The figure also shows the location of the Be star disc (parameters of the disc are found below from the analysis of the X-ray data). One can see that the set of observations denoted as X6–X10 enables to study the entrance to the disc in great details.

2.1 *XMM-Newton* observations

The log of the *XMM-Newton* data analysed in this paper is presented in Table 1. Observations X6–X10 were obtained as part of the 2004 periastron campaign and we have also used all other *XMM-Newton* observations of the system, which are now public (X1–X5). In the table, negative τ denotes the number of days before the date of 2004 periastron passage (2004 March 7), and positive values correspond to the number of days after the 2000 periastron (2000 October 17). θ is the orbital phase counted as shown in Fig. 1.

The *XMM-Newton* Observation Data Files (ODFs) were obtained from the online Science Archive;¹ the data were then processed and the event-lists filtered using *XMMSELECT* within the Science Analysis Software (SAS) v6.0.1. In all the observations, the source

¹ http://xmm.vilspa.esa.es/external/xmm_data_acc/xsa/index.shtml.

Table 1. Journal of *XMM–Newton* observations of PSR B1259–63.

Data set	Date	MJD	τ (d)	θ ($^{\circ}$)	Exposure (ks)
X1	2001-01-12	51921.73	87.2	320.8	11.3
X2	2001-07-11	52101.31	266.7	342.9	11.6
X3	2002-07-11	52467.24	–604.1	0.5	41.0
X4	2003-01-29	52668.27	–403.1	9.31	11.0
X5	2003-07-17	52837.53	–233.9	19.5	11.0
X6	2004-01-24	53028.79	–42.6	57.4	9.7
X7	2004-02-10	53045.43	–25.0	73.4	5.2
X8	2004-02-16	53051.39	–20.0	83.1	7.7
X9	2004-02-18	53052.02	–18.4	86.5	5.2
X10	2004-02-20	53055.82	–15.6	93.2	6.9

Table 2. Journal of *BeppoSAX* observations of PSR B1259–63.

Data set	Date	MJD	τ (d)	θ ($^{\circ}$)	Exposure (ks)
S1	1997-03-22	50529.63	–68.31	44.9	28.622
S2	1997-09-02	50693.75	95.81	322.9	16.985
S3	1997-09-08	50699.44	101.50	324.1	53.555
S4	1997-09-17	50708.08	110.14	325.9	51.301
S5	1997-09-25	50716.05	118.11	327.3	28.719

was observed with the MOS1 and MOS2 detectors. The X1–X5 observations were done in the Full Frame Mode, while the 2004 observations were performed in the Small Window Mode, to minimize the pile-up problems. For the X6–X10 observations, PN data are also available. In all the observations a medium filter was used.

The event-lists for spectral analysis were extracted from a 45-arcsec-radius circle at the source position for the X1–X5 observations, and from a 22.5-arcsec-radius circle for MOS1 and MOS2 observations in Small Window Mode (X6–X10). For the PN instrument, a region of 35 arcsec around the source position was chosen. Background photons were collected from a region located in the vicinity of the source with the same size area as the one chosen for the source photons.

For the spectral analysis, periods of soft proton flares need to be filtered out. To exclude them we have built light curves with a 100-s binning and excluded all time bins in which the count rate above 10 keV was higher than 1.5 cnt s^{-1} . The source countrate in 1–10 keV energy range varied from about 0.07 to 1.2 cts s^{-1} for MOS instruments, and from 0.4 to 4 cts s^{-1} for PN. Data from MOS1, MOS2 and, when available, PN detectors were combined in the spectral analysis to achieve best statistics.

2.2 *BeppoSAX* observations

Table 2 lists the observations of PSR B1259–63 made with *BeppoSAX* around the 1997 periastron passage. In the table, τ denotes the number of days before or after the 1997 periastron passage.

We used data from the Medium Energy Concentrator Spectrometer (MECS) instruments aboard *BeppoSAX* observatory which provides the coverage in the energy range ~ 1.5 –11.0 keV. Reduction of MECS data was done with the help of the standard tasks of LHEASOFT/FTOOLS v5.2 package according to the recommendations of *BeppoSAX* Guest Observer Facility.² Spectrum

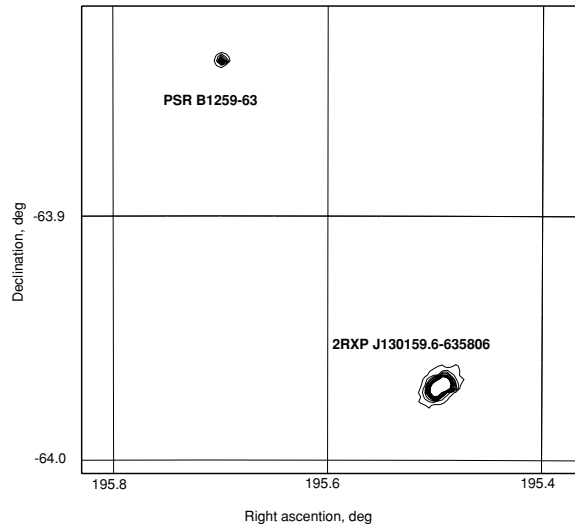


Figure 2. Contour plot of the *XMM–Newton* field of view for the X6 observation. A total of 10 contours were used with a linear scale between 5 cts pixel^{-1} (outer contour) and $50 \text{ cts pixel}^{-1}$ (inner contour). In this observation, 2RXP J130159.6–635806 was 40 times brighter than PSR B1259–63. This figure is taken from Chernyakova et al. (2005).

of the source was obtained extracting events from a circle of 3 arcmin radius around the source position. Spectrum of the instrument background was estimated considering events from a circle of the same radius 6 arcmin away from the source. Typically, the source provided several hundreds of counts per observation. Response matrices of MECS detectors were taken from NASA’s High Energy Astrophysics Science Archive Research Center (HEASARC) archive.³ Corrections of the photon’s arrival time to the Solar system barycentre for the subsequent usage of the event-lists in timing analysis were done with the help of tasks from SAXDAS package.⁴

We have checked that all the spectra obtained in the S2–S5 observations are consistent with each other, and combined them in order to improve statistics. We denote this combined spectrum as SC hereafter.

3 RESULTS

3.1 Imaging analysis

In the *XMM–Newton* field of view during its PSR B1259–63 observation programme, two sources were clearly detected [see Fig. 2 for the contour plot of *XMM–Newton* field of view for the MJD 53029 (X6) observation]. Besides PSR B1259–63 itself there is second source, which we have identified as 2RXP J130159.6–635806. Detailed analysis of this source is presented in Chernyakova et al. (2005). In this paper, it is shown, in particular, that 2RXP J130159.6–635806 is highly variable, with an intensity during flares which is several times larger than the peak intensity of PSR B1259–63. Therefore, although many observations of PSR B1259–63 have been made with *RXTE*, the fact that it is a non-imaging telescope means that it is extremely difficult to determine the flux from PSR B1259–63 alone. We therefore do not use numerous *RXTE* observations of the 2004 periastron passage, presented

² <http://heasarc.gsfc.nasa.gov/docs/sax/abc/saxabc/saxabc.html>,
<http://www.asdc.asi.it/bepposax/software/cookbook/>.

³ <http://heasarc.gsfc.nasa.gov/FTP/sax/cal/responses>.

⁴ <http://www.asdc.asi.it/bepposax/software/saxdas/index.html>.

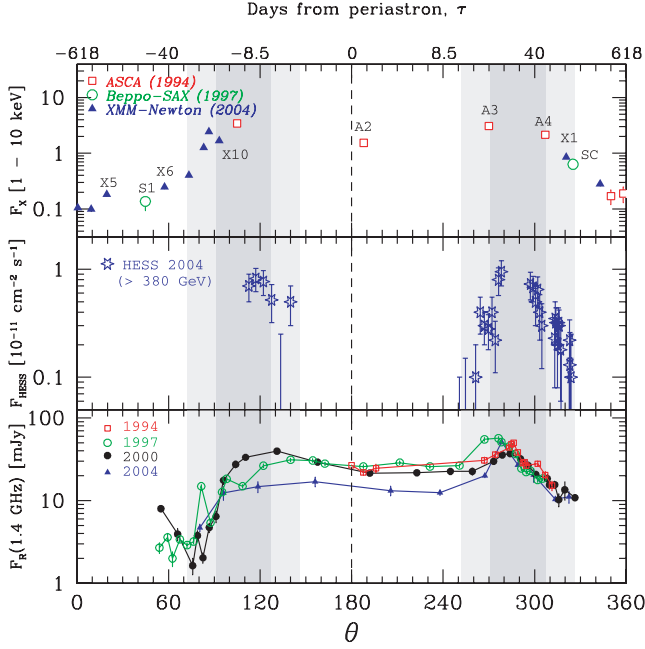


Figure 3. Comparison between the X-ray (top panel), TeV (middle panel) and radio (bottom panel) light curves. The 1–10 keV X-ray flux is given in $10^{-11} \text{ erg cm}^{-2} \text{ s}^{-1}$. The *XMM-Newton* observations are marked with triangles, *BeppoSAX* ones with circles, and *ASCA* ones with squares. Data for four different periastron passages are shown with different colours: red (1994), green (1997), black (2000) and blue (2004). x -axis (bottom panel) shows the orbital phase, θ , while x -axis (top panel) shows days from periastron, τ .

in Shaw et al. (2004). Note that despite in the Shaw et al. (2004) all *RXTE* observations are analysed, the authors were able to use in their analysis only data simultaneous to the *INTEGRAL* observations, when it was clear that influence of 2RXP J130159.6–635806 is small.

3.2 The X-ray light curve

The upper panel of Fig. 3 shows the X-ray light curve of the system. For comparison we also show in the same figure TeV light curve of the 2004 HESS observation (Aharonian et al. 2005) and radio (Johnston et al. 1999; Connors et al. 2002; Johnston et al. 2005) light curves of different years' periastron passages.

The X-ray flux from the source, in agreement with previous observations, was observed to be highly variable. The 1–10 keV flux is at minimum near apastron (observation X3), and has maximum more than 20 times larger, 18 d before periastron (X9). During observations X5, X6 and X7, the intensity of the emission increased, as the pulsar approached periastron and the Be star disc. 5 d after X7 observation, the flux increased by a factor of 4. During the next 2 d the intensity continued to increase, and reached its peak value at X9. The next observation (X10) was done only 3 d later, and the observed flux was already one and a half times lower.

Comparison of X-ray and radio light curves shows that the X-ray flux from the system varies in a more regular way than the radio flux: the X-ray data points from different periastron passages lie more or less on the same curve. Rapid growth of the X-ray flux found in our *XMM-Newton* observations X6–X10 is correlated with the rapid growth of the unpulsed radio emission from the system. The growth of radio and X-ray flux at these phases can be attributed to the pulsar entering the Be star disc.

Unfortunately, TeV observations start somewhat later and it is not possible to see whether the TeV flux grows during the pre-periastron disc crossing. However, simple geometrical argument tells that the orbital phase θ at which the pulsar should enter the disc for the second time should be shifted by 180° relative to the first entrance. From Fig. 3, one can infer that the first pre-periastron entrance falls roughly between the phases $70^\circ < \theta < 110^\circ$. Thus, the pulsar has to enter the disc again between the phases $250^\circ < \theta < 290^\circ$. Surprisingly, one can clearly see from the middle panel of Fig. 3 that the TeV flux grows in this phase interval.

The growth rate of the X-ray flux between the phases $70^\circ < \theta < 110^\circ$ is remarkably close to the decrease rate at the phases $290^\circ < \theta < 340^\circ$. This enables us to make a conjecture that the observed decrease of the X-ray flux can be associated to the exit of the pulsar from the disc. To test this conjecture, we superimpose the pre-periastron X-ray and TeV light curves over the post-periastron light curves by shifting the phase of the post-periastron data points by -180° . For X-rays we have used only data from the rise ($\theta < 110^\circ$) and the fall ($\theta > 290^\circ$) periods. The result is shown in Fig. 4. One can see that in such representation the rise and decrease of both X-ray and TeV flux from the system can be well fitted with a Gaussian curve $F(\theta) \sim \exp(-(\theta - \theta_{\text{disc}})^2 / (2\Delta\theta_{\text{disc}}^2))$. We find that the best fit is achieved with the parameter choice $\theta_{\text{disc}} \simeq 109.1^\circ$, $\Delta\theta_{\text{disc}} \simeq 18.5^\circ$ (the coordinate $\Delta\theta$ along the x -axis of Fig. 4 is, in fact $\Delta\theta = \theta - \theta_{\text{disc}}$).

The most obvious explanation to the shape of the X-ray and TeV light curves shown in Fig. 4 is that pulsar crosses the thick disc with the half-opening angle $\Delta\theta_{\text{disc}}$. The 'middle' plane of the disc intersects the pulsar orbital plane along the line $\theta = (109.1^\circ \cup 289.1^\circ)$. The intersection of the disc with the above parameters with the pulsar orbital plane is shown schematically in Fig. 1 by a shaded area. Because of the exponential profile, the disc has no fixed boundary. Denser shading in Fig. 1 corresponds to the one opening angle of the disc, while lighter shading corresponds to two opening angles. The disc is also shown by the same shading in the Fig. 3. From this figure, one can see that although the disc appears quite symmetric in terms of the orbital phase θ , it is highly asymmetric in terms of the time τ which measures days from the periastron passage. For

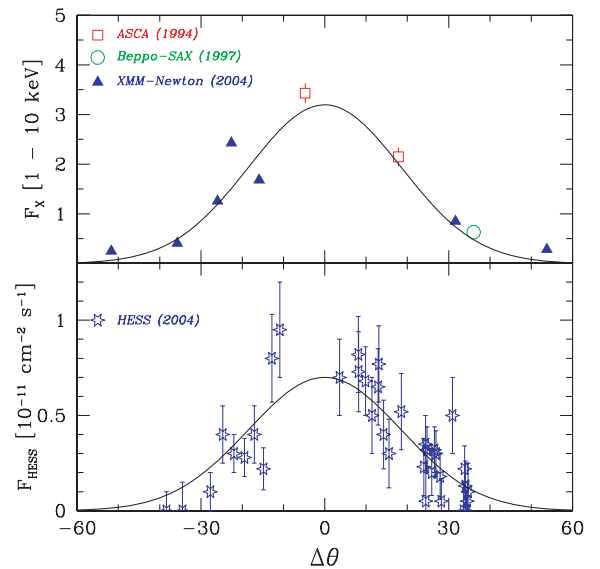


Figure 4. The X-ray (top panel) and TeV (bottom panel) flux as a function of the relative phase $\Delta\theta = \theta - \theta_{\text{disc}}$ (see text for the definition of θ_{disc}). The curves show a fit with a Gaussian of the half-width $\Delta\theta_{\text{disc}} = 18.5^\circ$.

example, during the second (post-periastron) disc passage, the rise phase ($250^\circ < \theta < 290^\circ$) of X-ray and TeV light curves takes just some 10 d, while the decay ($290^\circ < \theta < 340^\circ$) takes about 100 d.

3.3 Timing analysis

For each of the five PN event files in 0.2–10 keV energy range with a 6-ms time-resolution, we searched for a possible pulsation around the nominal 47.6-ms period using the epoch-folding technique (EFSEARCH tool from the XRONOS package). From the individual observations, the best 3σ upper limit on pulsation at a period of 47.6 ms is ~ 9 per cent, compatible with previous similar analysis made with ASCA (Kaspi et al. 1995; Hirayama et al. 1999). In order to perform a deeper search for pulsations, we combined neighbouring *XMM* observations (namely X7–X10, see. Table 1). As the time-span of these observations covers only small fraction of the binary orbit, we did not make corrections to the binary motion of the neutron star. Usage of the combined *XMM* data improves the upper limit to ~ 2 per cent.

Data of *BeppoSAX*/MECS (1.5–11 keV) observations also were searched for pulsations. For deeper search we combined observations S2–S5 (see Table 2). Due to small time-period of performed observations, we did not make correction for binary motion of the neutron star. In spite of considerably smaller effective area of MECS instruments of *BeppoSAX* observatory, the effective exposure time of observations of the source was much larger, which resulted in a comparable upper limit on X-ray pulsation fraction. We have not found pulsations with 3σ upper limit at ~ 2 per cent.

3.4 Spectral analysis

The spectral analysis was done with NASA/GSFC XSPEC software package. In Fig. 5, the folded and unfolded spectra of PSR B1259–63 for SC, X3, X6 and X9 observations are shown.

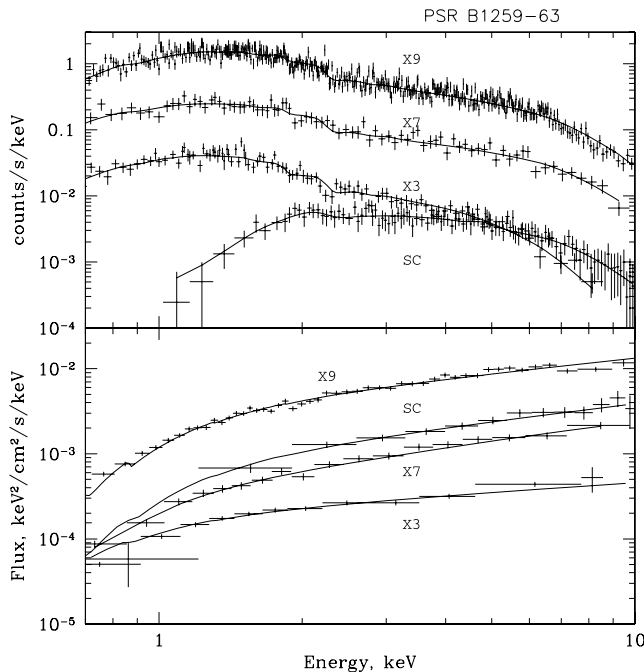


Figure 5. Folded (upper panel) and unfolded (bottom panel) PSR B1259–63 spectra from the SC, X3, X7, and X9 observations. The *XMM–Newton* spectra for X7 and X9 are for MOS1 instrument. The X3 spectrum is for PN instrument.

Table 3. Spectral parameters for *BeppoSAX* and *XMM–Newton* observations of PSR B1259–63.*

Data set	$F(1\text{--}10\text{ keV})$ $10^{-12}\text{ erg s}^{-1}$	Γ	N_{H} (10^{22} cm^{-2})	χ^2 (d.o.f.)
S1	$1.36^{+0.26}_{-0.43}$	$1.88^{+0.73}_{-0.22}$	$0.47^{+1.48}_{-0.47}$	0.814 (201)
SC	$6.31^{+0.69}_{-0.80}$	$1.39^{+0.06}_{-0.08}$	$0.65^{+0.16}_{-0.20}$	0.898 (813)
X1	8.51 (30)	1.51 (3)	0.45 (2)	0.97 (341)
X2	2.81 (23)	1.36 (7)	0.39 (4)	1.02 (122)
X3	1.04 (49)	1.69 (4)	0.29 (2)	0.88 (207)
X4	1.82 (14)	1.82 (7)	0.36 (3)	1.01 (109)
X5	0.99 (9)	1.80 (8)	0.32 (4)	0.80 (62)
X6	2.47 (17)	1.41 (6)	0.35 (3)	0.96 (151)
X7	4.05 (23)	1.20 (4)	0.28 (3)	0.95 (154)
X8	12.59 (34)	1.31 (2)	0.47 (1)	1.12 (614)
X9	24.27 (56)	1.39 (2)	0.43 (1)	1.07 (737)
X10	16.79 (37)	1.47 (2)	0.45 (1)	0.88 (772)

*Numbers in parentheses represent 68 per cent confidence interval uncertainties in the last digit quoted.

A simple power law with a photoelectrical absorption describes the data well, with no evidence for any line features. In Table 3, we present the results of the three parameter fits to the *XMM–Newton* data in the 0.5–10 keV energy range. The uncertainties are given at the 1σ statistical level and do not include systematic uncertainties. The graphical representation of the evolution of the PSR B1259–63 spectral parameters along the orbit is given in Fig. 6 which includes data from the *BeppoSAX* and *XMM–Newton* observations, and those from ASCA [taken from Hirayama et al. (1999)].

In Fig. 7, we show contour plots of N_{H} versus photon spectral index Γ , holding the 1–10 keV flux fixed at the values given in Table 3. The contours plotted are the 68, 90 and 99 per cent confidence levels. For the X5 observation, the values of N_{H} and Γ are consistent with X4 observation, and we omitted the X4 contours to keep the figure clear.

One can see that the variation of N_{H} as a function of orbital phase is correlated with the Be star disc crossing. No variations of N_{H} are observed for the *XMM–Newton* observations X2–X7 which all fall outside the disc (assuming the disc parameters found in Section 3.2). The mean value of N_{H} during these observations is $N_{\text{H}}(\text{X2–X7}) \sim 0.32 \times 10^{22}\text{ cm}^{-2}$. However, the observations X8, X9, X10 and X1 are characterized by absorption which is higher by a factor of about 1.5, $N_{\text{H}}(\text{X8–X10, X1}) \sim 0.45 \times 10^{22}\text{ cm}^{-2}$. Thus, the hydrogen column density remains high starting from about 20 d before the periastron till at least 87 d after periastron.

The behaviour of the spectral slope as a function of the orbital phase θ found in the *XMM* observations differs from the one found in the ASCA observations. Whereas in 1994–95 the spectrum at apastron was found to be significantly harder than during periastron, the *XMM–Newton* observations show much softer spectrum at the apastron with the spectral slope close to the ASCA periastron value.

The most remarkable feature of the spectral evolution of the system is the hardening of the X-ray spectrum close to the moment when pulsar enters the Be star disc at the phase $\theta \simeq \theta_{\text{disc}} - 2\Delta\theta_{\text{disc}} \simeq 70^\circ$. One can see that the decrease of the photon index Γ is simultaneous with the onset of the rapid growth of the X-ray flux. To the best of our knowledge, such behaviour was not predicted in any of existing models of X-ray emission from the system. Moreover, the observed values $\Gamma < 1.5$ during the observations X6–X10 are difficult to reconcile with the models of synchrotron or inverse-Compton emission from shock-accelerated electrons

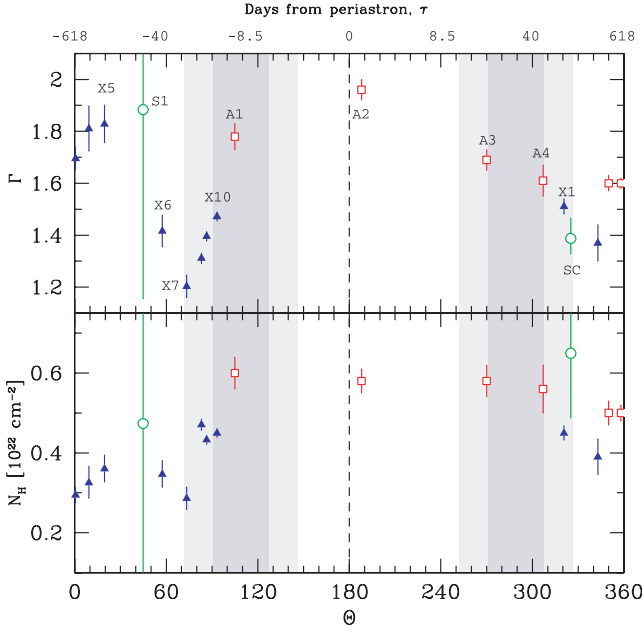


Figure 6. Spectral parameters of the *XMM-Newton*, *BeppoSAX*, and *ASCA* observations of the PSR B1259–63 system. Notations are the same as in Fig. 3. Top panel shows the evolution of the photon index Γ as a function of the orbital phase θ . Bottom panel shows the evolution of the hydrogen column density N_H . Denser and lighter shaded regions show phases within one and two half-opening angles of the Be star disc.

because of the too hard electron spectrum implied. Possible error in the determination of Γ due to the uncertainty in the determination of N_H (see Fig. 7) is too small to allow for $\Gamma \geq 1.5$ at least for observations X7–X9.

4 DISCUSSION

In all the theoretical models of unpulsed emission from PSR B1259–63, the collision of relativistic pulsar wind with non-relativistic wind of the Be star plays a crucial role. Due to the interaction of the winds, a system of two shock waves forms between the stars. Close to the Be star and to the pulsar, both winds are supposed to be radial but after passing the shocks, particles turn and start to flow along the contact surface, losing their energy via synchrotron and inverse-Compton (with the seed photons being the Be star soft photons) emission.

In the model of Chernyakova & Illarionov (1999, 2000) (CI), the observed X-ray emission is due to inverse-Compton scattering

of soft photons from the Be star on the same electron population that produce the non-pulsed radio emission from the system. The intensity of observed unpulsed X-ray and radio emission depends strongly on the flow velocity of the relativistic particles beyond the shock. Slower drift velocity leads to the higher concentration of the relativistic electrons beyond the shock and higher X-ray and radio luminosity. Decrease of the drift velocity during the pulsar passage through the disc is caused by the macroscopical mixing of pulsar wind with the stellar wind.

Main prediction of this model is the correlation of X-ray with the radio light curves of the system. Although different quality of X-ray and radio light curves does not allow to make definitive conclusions about radio–X-ray correlations, our *XMM-Newton* observations show that the onset of rapid increase of the X-ray flux is simultaneous with the appearance of the unpulsed radio emission from the system (see Fig. 3).

The X-ray inverse-Compton emission in the CI model is produced by electrons with rather moderate gamma-factors, $\gamma_{e,IC} \sim 10$, while the gamma-factors of radio-synchrotron-emitting electrons are around $\gamma_{e,s} \sim 10^2$. The synchrotron/inverse-Compton cooling times for such electrons are

$$t_s \simeq 10^8 \left[\frac{0.1 \text{ G}}{B} \right]^{3/2} \left[\frac{10 \text{ GHz}}{\nu} \right]^{1/2} \text{ s}, \quad (1)$$

and

$$t_{IC} \simeq 10^6 \left[\frac{1 \text{ erg cm}^{-3}}{U_r} \right] \left[\frac{1 \text{ keV}}{\epsilon_{IC}} \right]^{1/2} \text{ s}. \quad (2)$$

Both are large compared to the typical adiabatic cooling (or escape) time $t_{esc} \sim R/v \sim 10^3 \text{ s}$ (R is the characteristic size of the emission region, and v is the velocity of the flow along the contact surface). Another important time-scale for the electrons in the energy range relevant in the CI model is the Coulomb loss scale

$$t_{coulomb} \simeq 10^4 \left[\frac{10^9 \text{ cm}^3}{n} \right] \left[\frac{\gamma_e}{10} \right] \text{ s}. \quad (3)$$

As the pulsar enters the disc, the density of the stellar wind increases. Typical estimates of the wind density at the pulsar location [assuming the radial profile $n \sim (R_*/R)^2$] result in the density estimate $n \sim 10^9\text{--}10^{10} \text{ cm}^{-3}$. Thus, inside the disc, Coulomb cooling time is comparable to the escape time.

This effect leads to the modification of electron spectrum at the energies below the so-called ‘Coulomb break’ energy at which $t_{coulomb} = t_{esc}$:

$$\gamma_{e,coulomb} \simeq 1 \left[\frac{n}{10^9 \text{ cm}^{-3}} \right] \left[\frac{t_{esc}}{10^3 \text{ s}} \right]. \quad (4)$$

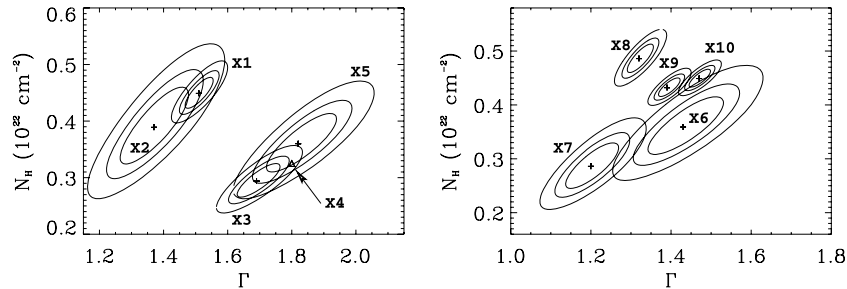


Figure 7. Confidence contour plots of the column density N_H and of the photon spectral index Γ uncertainties for a power-law fit to *XMM-Newton* observations. The contours give 68, 90 and 99 per cent confidence levels. X4 observation, marked with triangle, is very similar to the X5 observation and the contours are not plotted here.

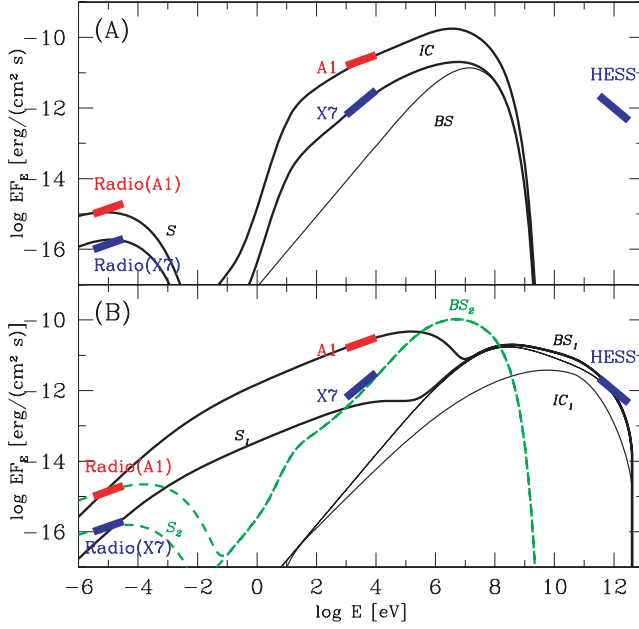


Figure 8. Modification of the broad-band spectra of CI (a) and TA (b) models due to the bremsstrahlung emission from shocked stellar/pulsar wind electrons during the disc passage. Contributions to the total spectrum from synchrotron, inverse-Compton and bremsstrahlung processes are marked with S, IC and BS, respectively. In the case of TA model, black solid curves show the spectrum of emission from the shocked pulsar wind, while the green dashed curves show the contribution from the shocked stellar wind. Parameters used for the CI model calculation are $n = 2 \times 10^9 \text{ cm}^{-3}$, $B = 0.01 \text{ G}$ (low) and $B = 0.1 \text{ G}$ (high synchrotron flux), and $dN_e/d\gamma \sim \gamma^{-2.4} \exp(-\gamma/400)$; with such parameters, Coulomb break is at $\gamma \sim 50$. The same parameters are used for the calculation of the shocked stellar wind emission (green dashed curves) in the lower panel. The emission from the shocked pulsar wind was calculated assuming $n = 2 \times 10^{11} \text{ cm}^{-3}$, $B = 0.15 \text{ G}$ (low) and $B = 1.5 \text{ G}$ (high synchrotron flux), and $dN_e/d\gamma \sim \gamma^{-2.3} \exp(-\gamma/4 \times 10^6)$. With such parameters, Coulomb break is at $\gamma \sim 500$.

Namely, since the Coulomb loss rate $dE/dt \sim \gamma_e/t_{\text{coulomb}}$ is energy-independent, the electron acceleration spectrum with the spectral index $\Gamma_e > 2$ hardens to $(\Gamma_e - 1) < 2$ below the break energy. This naturally leads to the hardening of the spectrum of inverse-Compton X-ray emission at the moment when the pulsar enters the disc, as it is shown in Fig. 8(a). One can note that the Coulomb break energy (3) is close to the energy of the X-ray emitting photons. This means that the X-ray photon index is very sensitive to the slight changes of the density and/or of the outflow velocity (see Fig. 8a in which the two spectra are calculated for $\gamma_{e,\text{coulomb}} = 10$ and 50). Since both vary during the disc passage (it is assumed that within the disc, pulsar and stellar winds are macroscopically mixed), numerical modelling is required to predict the time-evolution of the X-ray spectral index. We leave the detailed modelling of this for future work (Chernyakova & Neronov in preparation).

In the original CI model, only electrons with typical gamma-factors of 10–100 are considered. The presence of protons with comparable gamma-factors $\gamma_p \sim 1\text{--}10^3$ at the contact surface would lead to the generation of TeV emission during the disc passage which is due to the proton–proton interactions in the disc (see Kawachi, Naito & Patterson 2004). Macroscopic mixing of the pulsar and stellar wind will lead to the increase of the proton–proton interaction rate in the disc, which can explain the form of the TeV light curve of the system.

In the model of Tavani & Arons (1997) (TA), the X-ray emission is the synchrotron emission from shock-accelerated electrons of the pulsar wind. Typical gamma-factors of the X-ray emitting electrons are $\gamma \sim 10^6$. Modulation of the X-ray flux from the source during the disc and periastron passage is due to the combined effect of displacement of the contact surface by the disc (which leads to the variation of the magnetic field strength) and the increase of the inverse-Compton energy loss close to the periastron.

One of the main predictions of TA model is steepening of the X-ray spectrum during the disc and periastron passage. The effect is due to the fact that synchrotron and/or inverse-Compton cooling time of X-ray emitting electron becomes comparable or shorter than the time needed to escape from the emission region. However, the observed behaviour of the spectrum is quite opposite: the entrance to the disc is accompanied by the hardening of the spectrum.

The values of the photon index $\Gamma < 1.5$ found in the observations X6–X10 are too hard to be explained with the synchrotron emission from shock-accelerated electrons which normally result in the electron spectra with power-law index $\Gamma_e \geq 2$ and, correspondingly in synchrotron spectra with photon index $\Gamma \geq 1.5$. Of course, over a large fraction of the pulsar orbit, the synchrotron cooling time is larger than the time needed to escape from the emission region along the contact surface. Thus, if one assumes that the production spectrum of high-energy electrons responsible for the X-ray emission is harder than $\Gamma_e = 2$ (if, e.g. electrons originate in the cold pulsar wind with the bulk Lorentz factor $\gamma \sim 10^6$), then it is possible, in principle, to obtain spectra which are harder than $\Gamma = 1.5$. However, in this case one expects to observe the very hard X-ray spectrum with $\Gamma < 1.5$ over most of the pulsar orbit.

Within the TA model, radio synchrotron emission originates from different populations of electrons than the X-ray synchrotron emission (radio is conventionally attributed to shock-accelerated stellar wind electrons, while X-ray flux is emitted by the pulsar wind electrons). Although it is not possible to explain the hardening of the X-ray spectral index by the changes in the pulsar wind electron spectrum, one can try to ascribe the observed hardening to the contribution from the shocked stellar wind electrons. The X-ray spectrum with photon index harder than $\Gamma = 1.5$ is natural if there is a bremsstrahlung contribution to the X-ray flux. The increase of the density of stellar wind inside the disc can lead to the increase of bremsstrahlung luminosity.

The estimate of the bremsstrahlung loss time

$$t_{\text{brems}} = 10^5 \left[\frac{10^{10} \text{ cm}^{-3}}{n} \right] \text{ s} \quad (5)$$

shows that for radio-emitting electrons, it is orders of magnitude shorter than the synchrotron cooling time [see (1)]. Thus, the bremsstrahlung luminosity should be much higher than the radio synchrotron luminosity. From Fig. 8, one can see that a satisfactory fit to the broad-band spectrum can be obtained assuming the disc density $n \sim 10^{11} \text{ cm}^{-3}$. It is interesting to note that bremsstrahlung can also explain the behaviour of the TeV light curve in this case, if one assumes the possibility of mixing of the pulsar wind electrons with the pulsar disc medium (similar to the one assumed in the CI model).

The bremsstrahlung model faces, however, a serious overall energetics problem. From Fig. 8(b), one can see that the total bremsstrahlung luminosity is at least two orders of magnitude higher than the X-ray luminosity at the moment of X7 observation, $L_{X7} \simeq 10^{33} \text{ erg s}^{-1}$ (see Fig. 3). As it is discussed above, the energy-loss rate of mildly relativistic electrons responsible for the bremsstrahlung

emission is dominated by the Coulomb losses. Comparing (4) to (2), one can see that the Coulomb loss rate is still two to three orders of magnitude higher than the bremsstrahlung luminosity. Thus, to obtain the X-ray bremsstrahlung flux at the level of $10^{33} \text{ erg s}^{-1}$, one has to assume that the power injected into the 10–100 MeV electrons is about $10^{38} \text{ erg s}^{-1}$ which is much higher than the spin-down luminosity of the pulsar $L_{\text{pulsar}} \simeq 10^{36} \text{ erg s}^{-1}$.

5 CONCLUSIONS

In this paper, we have presented the *XMM-Newton* observations of the pulsar PSR B1259–63 during its 2004 periastron passage near the companion Be star SS 2883. Combining our observations with the previous X-ray observations from *XMM-Newton*, *BeppoSAX* and *ASCA*, we produced the detailed light curve of the system over the wide range of the orbital phases.

Using the large X-ray data sample, we were able to constrain the geometry of the Be star disc. In particular, we have found that the half-opening angle of the disc (projected on the pulsar orbital plane) is $\Delta\theta_{\text{disc}} \simeq 18^\circ.5$ and that the line of intersection of the disc with the pulsar orbital plane is inclined at about 70° with respect to the major axis of the pulsar orbit.

Inspection of the X-ray and TeV light curves of the system has revealed correlation of the X-ray and TeV flux variations. Our analysis shows that the variations of the TeV flux some 10–100 d after the periastron passage can be well fitted with the Gaussian curve whose parameters coincide with the parameters of the disc found from the X-ray analysis (centre at $\theta_{\text{disc}} = 289^\circ.1$, half-width $\Delta\theta = 18^\circ.5$) (see Fig. 4). If the observed behaviour of the flux is indeed due to the influence of Be star disc, then it cannot be explained within the inverse-Compton scattering model of TeV emission from the system.

Our *XMM-Newton* observations which were done during the period of first pulsar entrance to the disc (some 40 to 20 d before the periastron) revealed quite unexpected evolution of the spectrum of X-ray emission. In particular, the X-ray spectral slope hardened from $\Gamma \simeq 1.8$ down to $\simeq 1.2$ roughly at the onset of the rapid growth of the X-ray luminosity. This behaviour cannot be explained within the synchrotron model of X-ray emission from the system. We have shown that the observed hardening can be the result of the hardening of electron spectrum due to the Coulomb losses in the disc in the model where X-ray emission is the inverse-Compton emission from the population of electrons responsible for the radio synchrotron emission. Otherwise, the hardening can be caused by the increase of the bremsstrahlung emission from these electrons. However, the bremsstrahlung problem faces a serious energy balance problem.

ACKNOWLEDGMENTS

The authors acknowledge useful discussions with F. Aharonian and thank M. Revnivtsev for the help with the *BeppoSAX* data reduction. Authors are grateful to V. Kaspi for helpful comments. We are grateful to L. Foschini for helpful advices on the *XMM-Newton* data analysis. MC thanks M. Türler for the help with figure production. AL acknowledges the support of RFFI grant 04–02–17276.

REFERENCES

- Aharonian F. et al., A&A, 442, 1
- Ball L., Melatos A., Johnston S., Skjæraasen O., 1999, ApJ, 514, L39
- Chernyakova M., Illarionov A., 1999, MNRAS, 304, 359
- Chernyakova M., Illarionov A., 2000, ApSS, 274, 177
- Chernyakova M., Lutovinov A., Rodriguez J., Revnivtsev M., 2005, MNRAS, 364, 455
- Cominsky L., Roberts M., Johnston S., 1994, ApJ, 427, 978
- Connors T.W., Johnston S., Manchester R. N., McConnell D., 2002, MNRAS, 336, 1201
- Grove J. E., Tavani M., Purcell W. R., Johnson W. N., Kurfess J. D., Strickman M. S., Arons J., 1995, ApJ, 447, L113
- Hirayama M., Cominsky L. R., Kaspi V. M., Nagase F., Tavani M., Kawai N., Grove J. E., 1999, ApJ, 521, 718
- Johnston S., Manchester R. N., Lyne A., Bailes M., Kaspi V. M., Qiao Guojun, D’Amico N., 1992, ApJ, 387, L37
- Johnston S., Manchester R. N., Lyne A. G., Nicastro L., Spyromilio J., 1994, MNRAS, 268, 430
- Johnston S., Manchester R. N., McConnell D., Campbell-Wilson D., 1999, MNRAS, 302, 277
- Johnston S., Ball L., Wang N., Manchester R. N., 2005, MNRAS, 358, 1069
- Kaspi V. M., Tavani M., Nagase F., Hirayama M., Hoshino M., Aoki T., Kawai N., Arons J., 1995, ApJ, 453, 424
- Kawachi A., Naito T., Patterson J. R., 2004, ApJ, 607, 949
- Kirk J. G., Skjæraasen O., Gallant Y. A., 2002, A&A, 388, L29
- McClure-Griffiths N. M., Johnston S., Stinebring D. R., Nicastro L., 1998, ApJ, 492, L49
- Shaw S., Chernyakova M., Rodriguez J., Walter R., Kretschmar P., Mereghetti S., 2004, A&A, 426, L33
- Tavani M., Arons J., 1997, ApJ, 477, 439
- Taylor J. H., Manchester R. N., Lyne A. G., 1993, ApJS, 88, 529
- Wang N., Johnston S., Manchester R. N., 2004, MNRAS, 351, 599
- Waters L. B. F. M., van den Heuvel E. P. J., Taylor A. R., Habets G. M. H. J., Persi P., 1988, A&A, 198, 200
- Wex N., Johnston S., Manchester R. N., Lyne A. G., Stappers B. W., Bailes M., 1998, MNRAS, 298, 997

This paper has been typeset from a $\text{\TeX}/\text{\LaTeX}$ file prepared by the author.